09,08

Orthoborate $LiSrY_2(BO_3)_3$ Host with Low Concentration Quenching

© P.K. Tawalare[1], B.Y. Fugare[1], R.A. Nafdey[2], K. Sharma[3], S.V. Moharil[4]

[1] Department of Physics, Jagadamba Mahavidyalaya,
Achalpur City, 444806, India
[2] Shri Ramdeobaba College of Engineering and Management,
Nagpur, 440013, India
[3] Physics Department, Jhulelal Institute of Technology,
Nagpur, 441111, India
[4] RashtrasantTukadoji Maharaj Nagpur University,
Nagpur 440010, India

E-mail: aounyacine07@gmail.com

Received May 29, 2023
Revised May 29, 2023
Accepted June 6, 2023

$LiSrY_2(BO_3)_3$ is a recently explored host for observing lanthanide luminescence. This compound synthesized and activated with Tb^{3+}/Gd^{3+} is described. Trivalent activators Tb^{3+} and Gd^{3+} occupy yttrium sites. Intense characteristic emission is observed for both these activators. In case of Gd^{3+}, both excitation and emission lines arise in f−f transitions. Photo luminescence emission is obtained in UV region. In case of Tb^{3+}, mild concentration quenching was observed above 10%. Prominent excitation of Tb^{3+} is in form of a band arising in f−d type transition while emission comes from f−f transitions. Emission lifetimes are of the order of milliseconds, typical of forbidden f−f transitions.

Keywords: photoluminescence; borate; Gd^{3+}; Tb^{3+}.

DOI: 10.61011/PSS.2023.08.56581.92

1. Introduction

Boron is commonly found element in the nature. Its reactivity with almost all other elements is superb. It forms compounds along with oxygen and the metals termed as borates. The different borates are formed with different anions like BO_3^{3-}, $B_2O_5^{4-}$, *etc.* Many of these borates occur as minerals. More than 100 such structures are known. *E.g.* „huntites“ are a class of borate compounds with general formula $RM_3(BO_3)_4$. Here, R =Ln and Y while M =Al, Fe, and Ga. These have been of interest due to various properties like „acoustic-electric, piezoelectric, luminescent, magnetic properties, ferroelectrics *etc.* they exhibit“ [1]. To combine the simplicity of borate synthesis with superior properties of lanthanides, several synthetic borates involving lanthanide ions have been explored. Borate chemistry is so rich that newer and newer compositions are still being discovered. $K_5Mg_2La_3(BO_3)_6$ [2], $K_7CaY_2(B_5O_{10})_3$ [3], $KSrY(BO_3)_2$ [4], $Sr_3Gd_2(BO_3)_4$ [5], $CsBaYB_6O_{12}$ [6], $LiCaGd_5(BO_3)_6$ [7], $LiCaY_5(BO_3)_6$ [8] are among such recently explored compositions.

$LiSrY_2(BO_3)_3$ is another such borate reported by Song *et al.* about a decade back [9]. Subsequently, Chen *et al.* prepared isostructural borate series involving almost all the lanthanides excluding lanthanum and cerium [10]. Luminescence of stoichiometric Tb compound was also described by these authors. This is rather surprising. Tb−Tb distance is about 3.677 Å in $LiSrTb_2(BO_3)_3$, and one would expect concentration quenching due to Tb−Tb energy transfer. He *et al.* [11] studied luminescence of Eu^{3+} in $LiSrY_2(BO_3)_3$ host. They observed concentration quenching setting in at the value as high as 70%.

It will be thus interesting to study luminescence properties of various activators in this host noting subdued concentration quenching. Such studies may provide insight into the mechanism of the concentration quenching or absence thereof, as well as some new phosphors with remarkable luminescence characteristics. Here, we report luminescence of Tb^{3+} and Gd^{3+} in $LiSrY_2(BO_3)_3$ host.

2. Experimental

Synthesis and characterization details are similar to those published earlier. In short, $LiSrY_2(BO_3)_3$ was produced by reacting the ingredients in solid state. The Analar grade reagents $SrCO_3$, Y_2O_3, Li_2CO_3, and H_3BO_3 were used. The ingredients were mixed in stoichiometric proportions except H_3BO_3 which was used in 10% excess to compensate for evaporation losses during the synthesis, and the desired amount of activator oxides (Gd_2O_3/Tb_4O_7) were added during this process. The mixtures were heated in the high-temperature muffle furnace. Various phosphors with Tb^{3+}/Gd^{3+} concentration varying between 1−20% relative to Y were prepared. Two-step heating was used. In the first step, heating was done at 400°C for 6 hours to decompose carbonates/nitrates to oxides. Thereafter the temperature was raised to 780°C and compound was kept at 12 hours.

Samples were then slowly cooled by switching off the furnace. At room temperature, the samples were removed from the furnace. The sample was crushed to obtain powder of dimensions ($< 30\,\mu$m). This powder was then used in the subsequent experiments.

The record of X-ray diffraction patterns was done on Philips PANalytical X'pert Pro diffractometer. Photoluminescence characteristics and reflectance spectra ($BaSO_4$ as standard) were measured using a Model Hitachi F-7000 spectroluorimeter in the range of 200–700 nm. Lifetime measurements were also done by using same instrument operating in time mode. Electron micrograph and elemental mapping was obtained using Model JEOL JSM 6380A scanning electron microscope, with Bruker attachment.

3. Results and discussion

Fig. 1, *a* depicts X-ray diffraction (XRD) pattern of $LiSrY_2(BO_3)_3$ prepared as described above. A comparison is made with the XRD pattern calculated by Vesta software [12]. Two patterns bear a close resemblance. Thus, phase-pure $LiSrY_2(BO_3)_3$ is formed. The obtained XRD pattern was refined using Fullprof software. The results are shown in Fig. 1, *b*. Goodness-of-fit-parameters are: profile residual factor $R_p = 6.71$, weighted profile residual $R_{wp} = 8.34$ and $\chi^2 = 1.21$. Value of χ^2 close to 1 again indicate formation of phase-pure $LiSrY_2(BO_3)_3$. Other relevant refinement parameters are space group P-3 m1, $a = 10.33$ Å, $c = 6.39$ Å, and $Z = 3 \cdot \text{cell.vol} = 590.516$ Å^3. Atomic coordinates are listed in the Table.

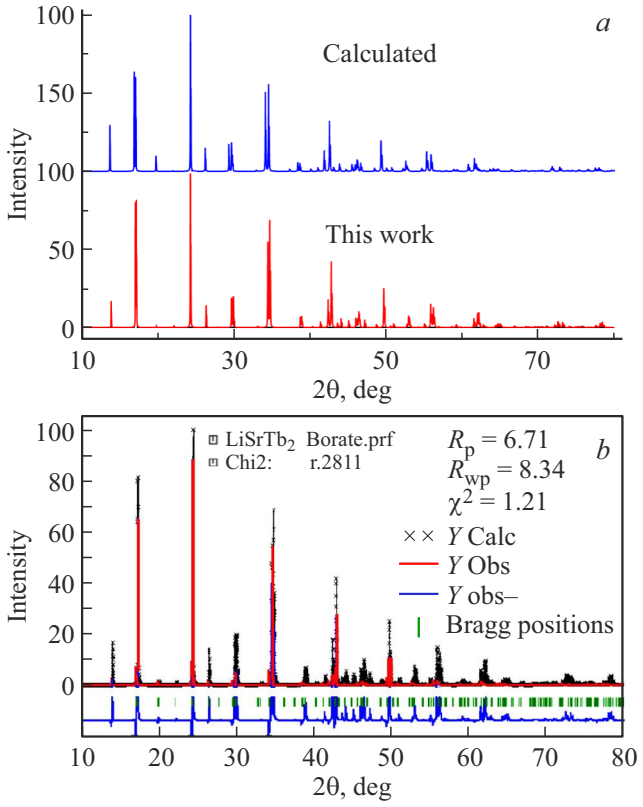

Figure 1. *a*) XRD pattern of $LiSrY_2(BO_3)_3$ compared with calculated patterns. An excellent match is seen. *b*) Rietveld refinement of the XRD pattern.

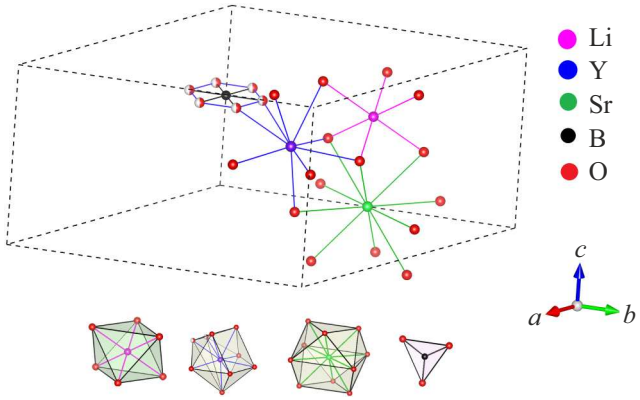

Figure 2. Unit cell of $LiSrY_2(BO_3)_3$ showing cation coordination and coordination polyhedra.

$LiSrY_2(BO_3)_3$ unit cell comprises 10 crystallographically different atoms. These atoms are Li, Sr, O(1), O(2), O(3), O(4), B(1), B(2), B(3), and Tb. Occupancy is 1 indicating specific positions. The only exception is O(4) which has occupancy of 0.5. Tb is 8-coordinated. TbO_8 coordination polyhedron (Fig. 2) is formed by Tb–O having distances ranging between 2.28 to 2.46 Å. Six such polyhedra are joined by either a common edge or common face. This results in a hexagonal $[Tb_6O_{33}]$ configuration in the direction of *c*-axis. In turn, two such configurations are joined at corners leading to a layer perpendicular to *c*-axis. In this layer trigonal, hexagonal, and rhombic tunnels are formed. The first two tunnels are engaged by the triangular B(1)O3 and B(3)O3 groups, respectively. A distorted LiO_6 octahedra reside in the rhombic tunnels.

Fractional atomic coordinates for $LiSrY_2(BO_3)_3$

Element	*x*	*y*	*z*
Tb	0.177090	0.822910	0.358180
Sr	0.000000	0.500000	0.000000
O1	0.179600	0.589800	0.333333
O2	0.626000	−0.301400	0.690600
O3	0.197800	0.802200	0.010000
O4	0.124000	0.124000	0.500000
B1	0.333333	0.666667	0.331000
B2	0.189600	0.810400	−0.196500
B3	0.000000	0.000000	0.500000
Li1	0.000000	0.500000	0.500000

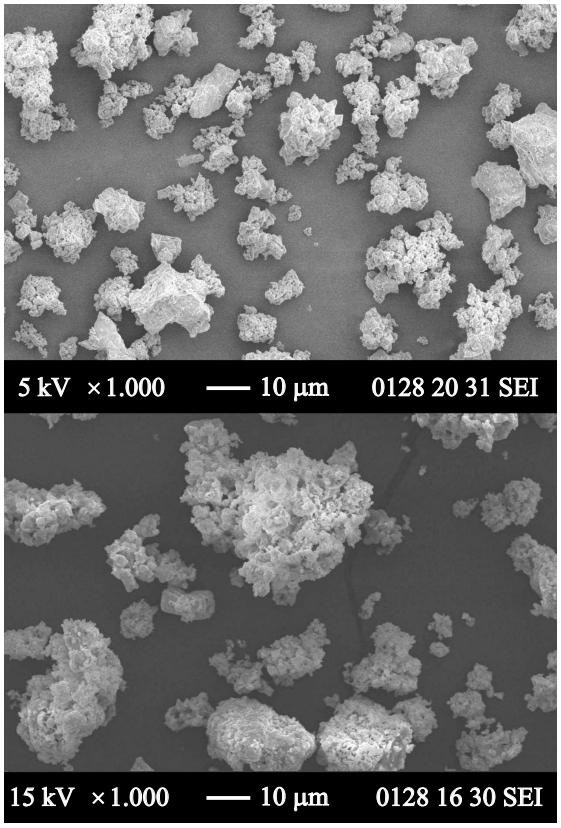

Figure 3. Electron micrographs.

Essentially, the Tb_6O_{33} layer is strengthened by joining with B(1)O3 group, B(3)O3 group, and LiO6 groups. The three-dimensional structure is completed by bridges in form of B(2)O3 groups. Sr atoms are ten-coordinated. They are in the interstices between these polyhedral layers. They look like stitches connecting various layers [10].

Electron micrographs are presented in Fig. 3. From the micrograph of the sample, it can be seen that the powders obtained by the solid-state method are characterized by particles of irregular shape. The size of the particle is within the range of $5-25\,\mu$m. For confirming the homogeneous distribution of the elements, elemental mapping was done and the results are presented in Fig. 4. These results confirm that the elements are uniformly distributed.

Fig. 5 shows reflectance spectra for $LiSrY_{1.6}Tb_{0.4}(BO_3)_3$ phosphor. Tb^{3+} will obviously enter at yttrium site; Al being too small and Sr is divalent. Both reflectance and Kubelka–Munk functions are plotted against wavelength. The latter is more closely linked to absorption. A prominent absorption band is seen around 260 nm. This is due to interconfigurational transition between states of $4f^8$ and $4f^75d^1$ configurations.

Results for photoluminescence emission spectra of $LiSrY_2(BO_3)_3$ activated with Tb^{3+} are presented in Fig.6. Emission spectrum obtained with 236 nm contains typical lines at 381 ($^5D_3 \rightarrow {}^7F_6$), 415 ($^5D_3 \rightarrow {}^7F_5$), 488, 499 ($^5D_4 \rightarrow {}^7F_6$), 545, 553 ($^5D_4 \rightarrow {}^7F_5$), 587, 592 ($^5D_4 \rightarrow {}^7F_4$), and 621 ($^5D_4 \rightarrow {}^7F_3$) nm. Intensities of the green emission lines around 545 nm goes on increasing with Tb^{3+} concentration (Fig. 6, inset). The highest intensity is observed for 10 mol.%. A slight decrease is registered for higher values indicating marginal concentration quenching. In $LiSrY_2(BO_3)_3$, Y–Y distance is 3.651 Å. This is much shorter than 5 Å. The reason for concentration quenching is this short Y–Y distance expected due to $RE^{3+}-RE^{3+}$ energy transfer. This can be attributed to concentration quenching. From this data, critical distance associated with $Tb^{3+}-Tb^{3+}$ energy transfer can be calculated using Blasse's formula [13].

The critical distance is elaborated as the distance for which the transfer and emission probability equals. Qualitatively, it gives the idea about the closeness of ions and the distance R_c up to which ions can come close without influencing each other.

$$R_c = 2\left(\sqrt[3]{\frac{3V}{4\pi x_c N}}\right)$$

Here, x_c =critical concentration (0.1), N = number of Y sites in the unit cell (6), V = volume of the unit cell (590.516 Å^3), calculated $R_c = 12.34$ Å. When the energy transfer mechanism is dipole–dipole, the critical distance is of the 5 Å order. Thus the interaction between dipole–dipole is not responsible for the concentration quenching as R_c value is 12.34 Å (> 5 Å).

Emission colour of Tb^{3+} is green. The colour coordinates were obtained using GoCIE [14] program. The values calculated for $LiSrY_{1.6}Tb_{0.4}(BO_3)_3$ are $x = 0.27$, $y = 0.56$ (Fig. 7). These are close to EBU PAL/SECAM green standard ($x = 0.29$, $y = 0.60$).

In the excitation spectrum (Fig. 8), a broad band can be seen around 261 nm and another weaker one at 290 nm. This is the same as that observed in the reflectance spectra of Fig. 5. These bands arise from the so-called f–d transitions. The ground state $^7F_6$ of the Tb^{3+} belongs to ($4f^8$) configuration. Highest excited states arise from $4f^75d^1$ configuration. These are classified as high-spin ^9D_J state and the ^7D_J low-spin state. ^9D_J states are lower in energy. Transitions between ^7F_J and ^7D_J are (higher energy) spin-allowed. Transitions between ^7F_J and ^9D_J are (lower energy) spin-forbidden. The 238 and 282 nm bands thus arise from the transitions from $^7F_6$ ($4f^8$) state to the ^7D_J ($4f^75d^1$) states. Apart from this, sharp lines appear at longer wavelengths. The longer wavelength lines are attributable to f–f transitions of Tb^{3+}. These are located at 316 ($^7F_6 \rightarrow {}^5D_1$), 340 ($^7F_6 \rightarrow {}^5L_6$), 351 ($^7F_6 \rightarrow {}^5D_2$), 366 ($^7F_6 \rightarrow {}^5L_{10}$), 377 ($^7F_6 \rightarrow {}^5G_6$), 426 ($^7F_6 \rightarrow {}^5D_3$), and 488 nm ($^7F_6 \rightarrow {}^5D_4$). Fig. 9 shows the various transitions involved in emission, excitation spectra of Tb^{3+} in $LiSrY_2(BO_3)_3$ host.

Fig. 10 shows luminescence decay curves for $LiSrY_{1.98}Tb_{0.02}(BO_3)_3$ and $LiSrY_{1.6}Tb_{0.4}(BO_3)_3$ phosphors.

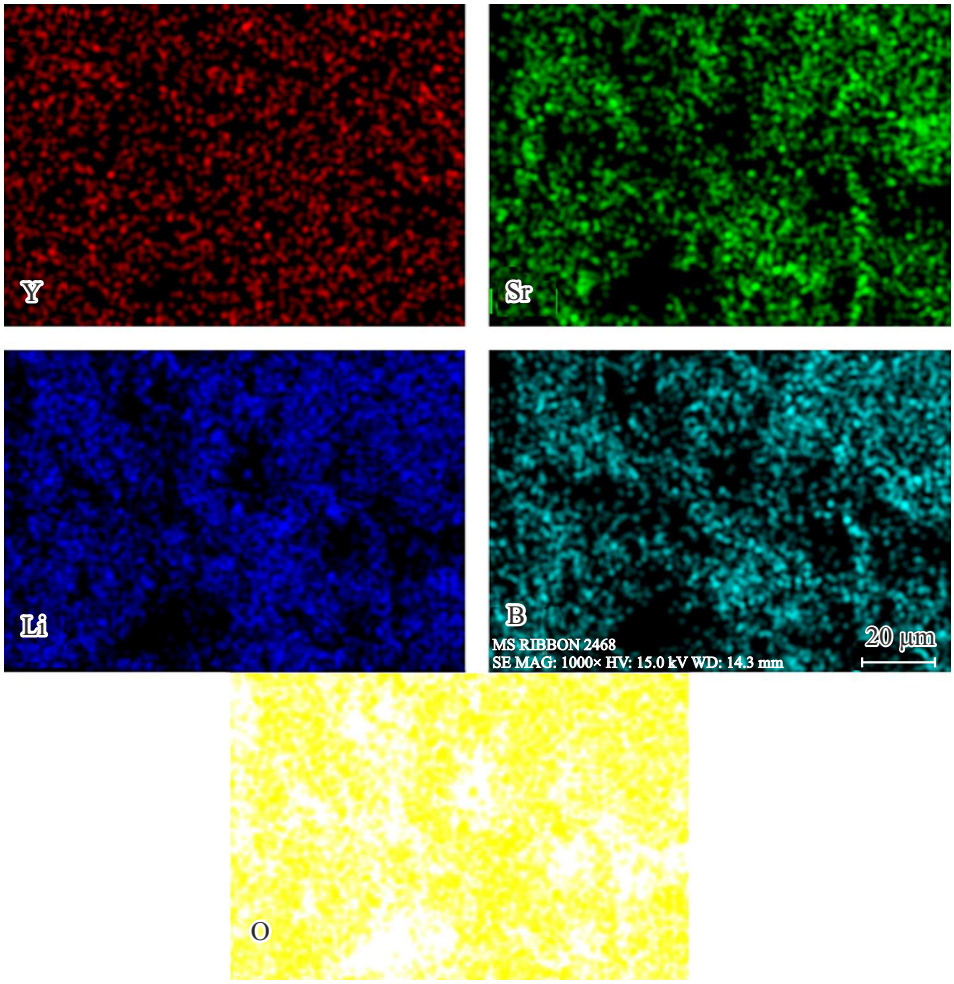

Figure 4. Elemental mapping.

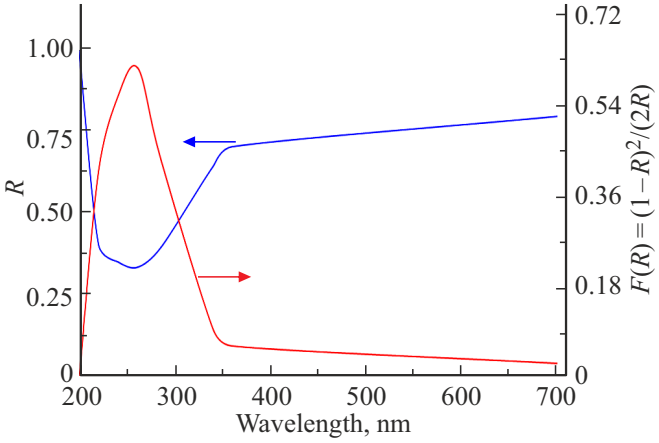

Figure 5. Reflectance spectra of $LiSrY_{1.6}Tb_{0.4}(BO_3)_3$ phosphor. Both reflectance (right-hand side ordinate) and Kubelka–Munk functions (left-hand side ordinate) are plotted against wavelength.

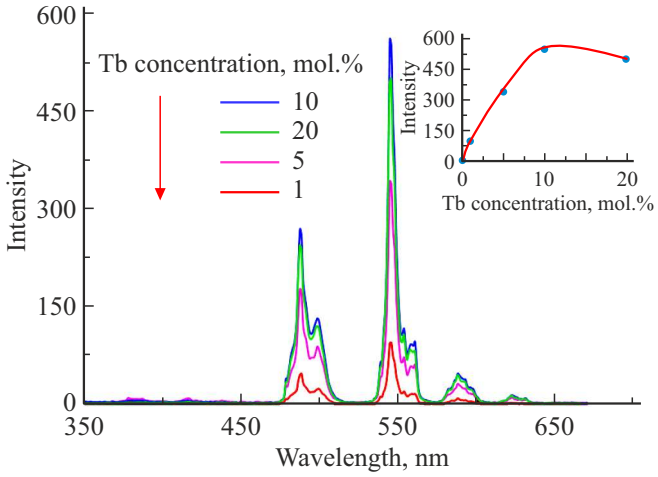

Figure 6. PL emission spectra for Tb^{3+} activated $LiSrY_2(BO_3)_3$. 261 nm was used for excitation. The inset shows the concentration dependence of the intensity of 545-nm emission.

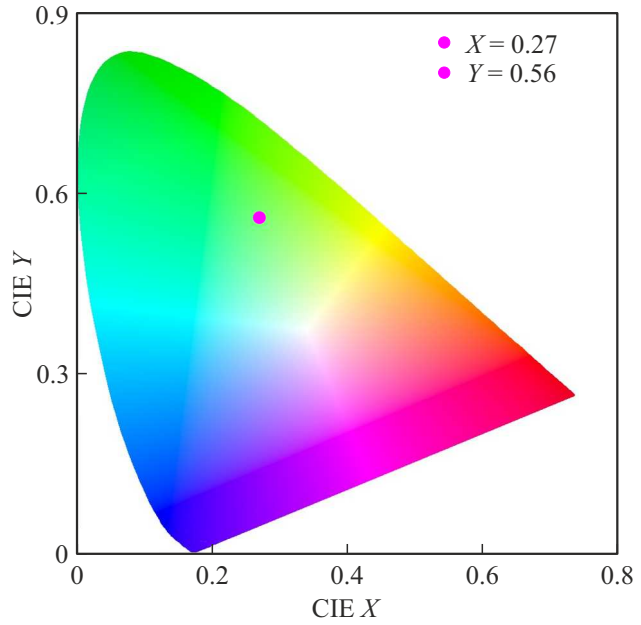

Figure 7. Colour coordinates for $LiSrY_{1.6}Tb_{0.4}(BO_3)_3$ phosphor.

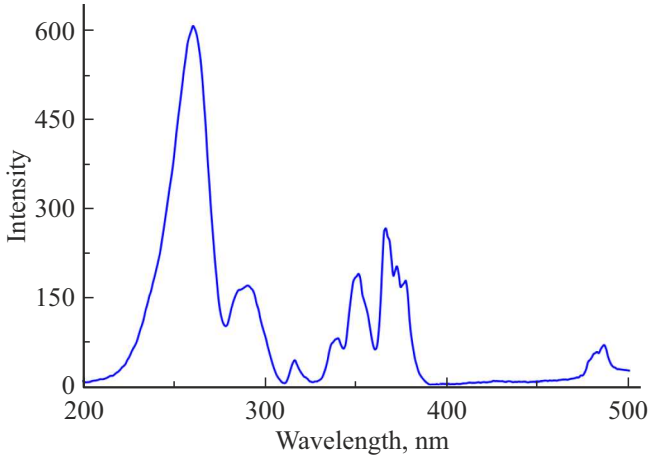

Figure 8. PL excitation spectra for Tb^{3+} activated $LiSrY_2(BO_3)_3$. Monitored wavelength 545 nm.

Decay was recorded for 545-nm emission. 261-nm excitation was used. Decay curve is fitted as a nature of single exponential. For $LiSrY_{1.98}Tb_{0.02}(BO_3)_3$, the lifetime was obtained as $\tau = 2.55$ ms. Decay becomes slightly faster with increasing concentration. For $LiSrY_{1.6}Tb_{0.4}(BO_3)_3$, the decay could be fitted to $\tau = 2.33$ ms. Only a marginal decrease in lifetime is consistent with moderate concentration quenching.

Photo luminescence (PL) emission was observed for $LiSrY_2(BO_3)_3$ phosphors containing Gd^{3+} activator (Fig. 11). Upon 274-nm excitation, typical line emission is seen. A very intense line is at 313 nm. The weaker lines are also observed at 307 and 325 nm. The longer wavelength emission could be due to vibronic transition. The emissions at 307 and 313 nm arise in $^6P_J \rightarrow {}^8S_{7/2}$ transitions. Intensity of the 313-emission goes on increasing with Gd^{3+} concentration (Fig. 11, inset) up to 5% and then marginal decrease is seen.

In the excitation spectrum (Fig. 12), the most intense line is at 274 nm with some structure. This is due to $^8S_{7/2} \rightarrow {}^6I_J$ transitions. There are also weak lines at shorter wavelengths around 247 and 253 nm. These are due to transitions to higher energy levels $^4D_{3/2}$. Fig. 13 shows the various transitions involved in the excitation and emission spectra of Gd^{3+} in for $LiSrY_2(BO_3)_3$ host. The excitation at 274 nm takes Gd^{3+} to the excited states ^6I_J. From there, it relaxes to ^6P_J states by emitting phonons. The transitions to ground state $^8S_{7/2}$ results in emissions at 307 and 313 nm.

Fig. 14 shows results of lifetime measurements for $LiSrY_{1.98}Gd_{0.02}(BO_3)_3$ and $LiSrY_{1.6}Gd_{0.4}(BO_3)_3$ phosphors. Decay was recorded for 313-nm emission. 274-nm excitation was used. For $LiSrY_{1.98}Gd_{0.02}(BO_3)_3$, lifetime is 4.20 ms. It is 3.75 ms for $LiSrY_{1.6}Gd_{0.4}(BO_3)_3$.

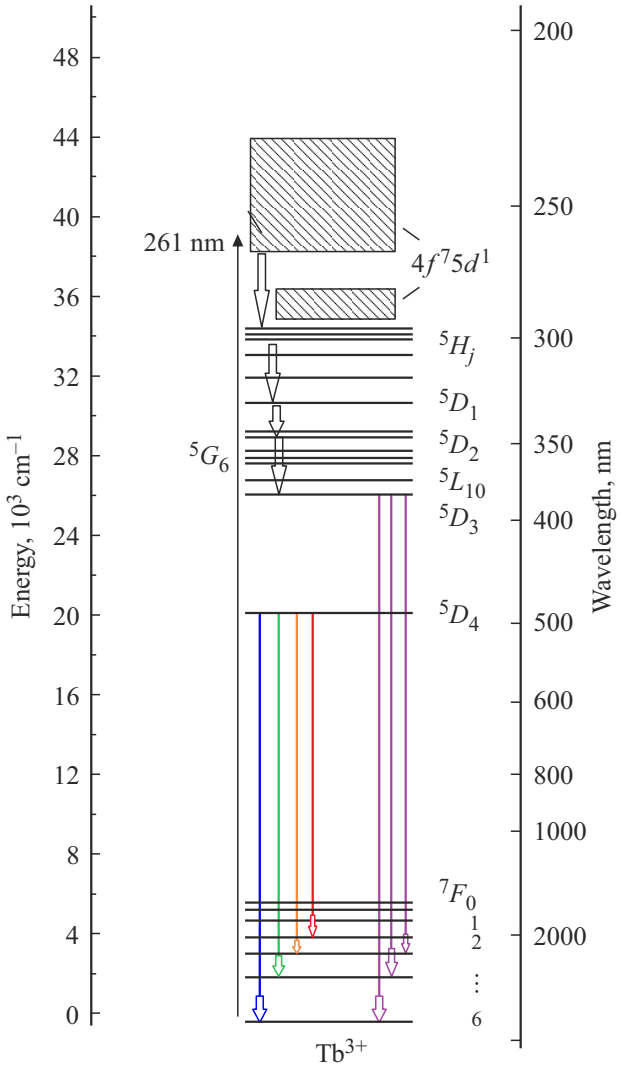

Figure 9. Energy level diagram showing the various transitions involved in the excitation and emission spectra of Tb^{3+} in for $LiSrY_2(BO_3)_3$ host.

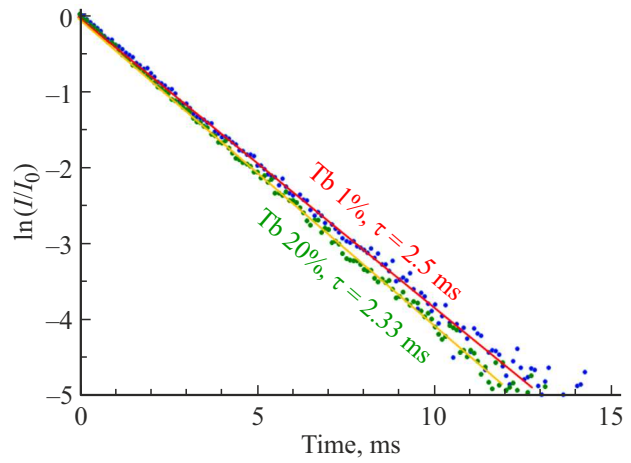

Figure 10. Luminescence decay curve for $LiSrY_{1.98}Tb_{0.02}(BO_3)_3$ and $LiSrY_{1.6}Tb_{0.4}(BO_3)_3$ phosphor. Decay was recorded for 545 nm emission. 261 nm excitation was used.

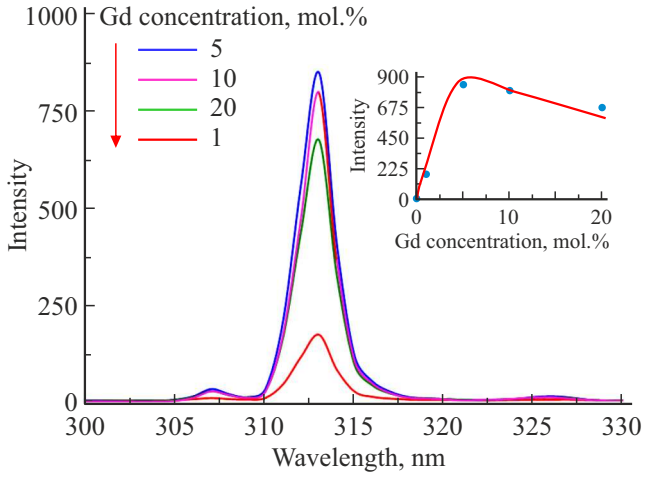

Figure 11. PL emission spectra for Gd^{3+} activated $LiSrY_2(BO_3)_3$. Inset shows the concentration dependence of 313-nm emission.

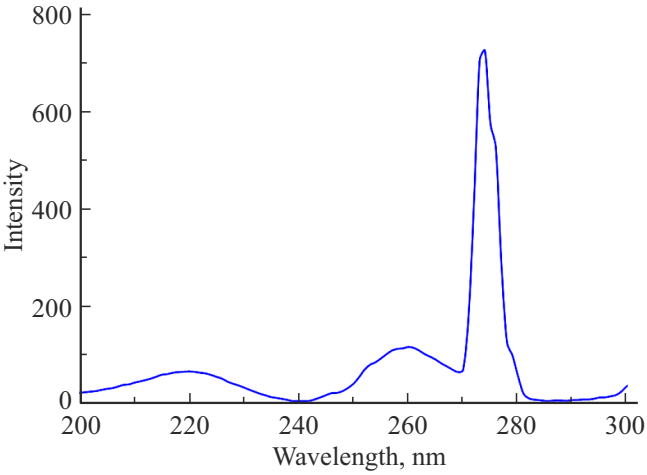

Figure 12. PL excitation spectra for Gd^{3+} activated $LiSrY_2(BO_3)_3$.

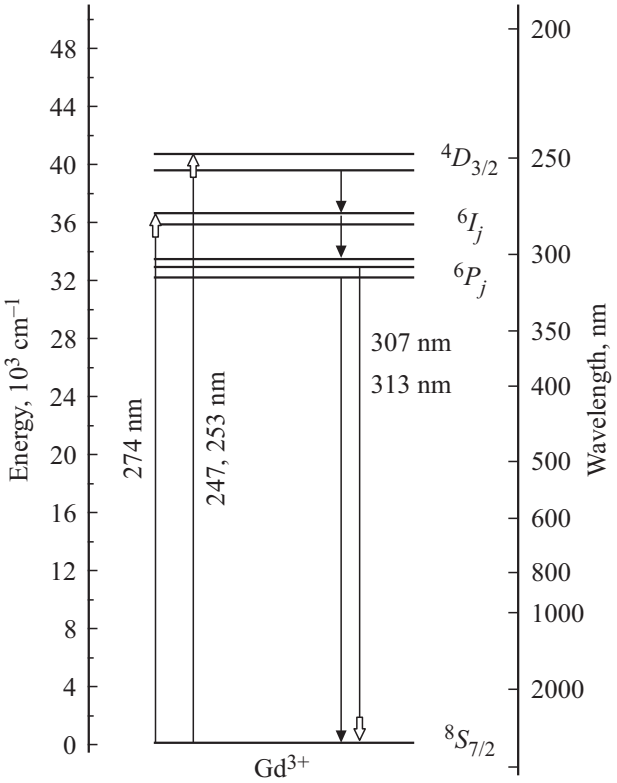

Figure 13. Energy level diagram showing the various transitions involved in the excitation and emission spectra of Gd^{3+} in for $LiSrY_2(BO_3)_3$ host.

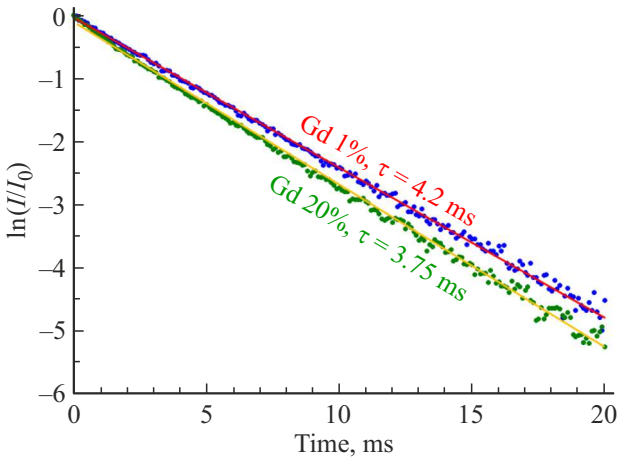

Figure 14. Lifetime measurements for $LiSrY_{1.9}8Gd_{0.02}(BO_3)_3$ and $LiSrY_{1.6}Gd_{0.4}(BO_3)_3$. Decay was recorded for 313-nm emission. 274-nm excitation was used.

Reduction in decay time can be due to energy transfer among Gd^{3+} ions.

4. Conclusions

Intense emission from Gd^{3+} and Tb^{3+} lanthanide activators was obtained in the $LiSrY_2(BO_3)_3$ host. Tb^{3+}

emission is green with the colour coordinates ($X = 0.27$, $Y = 0.56$). Both f−d and f−f excitations lead to this emission. Moderate concentration quenching is noticed above 10%. Gd^{3+} gives characteristic UVB emission at 313 nm which can be excited by a f−f line at 274 nm. Lifetimes are of the order of few ms expected of f−f transitions. Moderate concentration quenching is useful for obtaining high emission intensities. $LiSrY_2(BO-3)_3$ host may prove useful for obtaining phosphors based on other activators as well.

Authors' contrbution

P.K. Tawalare has provided the concept and material synthesis while R.A. Nafdey and K. Sharma have helped in manuscript preparation and B.Y. Fugare and S.V. Moharil in editing.

Acknowledgements

P.K. Tawalare is thankful to the Head of the Department of Physics, thankful to the Jagadamba Mahavidyalaya Achalpur for their constant support. Rietveld refinement was carried out using Full prof software. Crystal structure diagrams are prepared with Vesta and colour coordinates are plotted using GoCIE. The authors are grateful to the developers for permitting free use of these software.

Conflicts of interests

Authors declare no conflict of interest.

References

[1] P.K. Tawalare. Lumin. **37**, *8*, 1226 (2022). https://doi.org/10.1002/bio.4301
[2] R. Liu, H. Wu, H. Yu, Z. Hu, J. Wang, Y. Wu. Chem. Mater. **33**, *11*, 4240 (2021). https://doi.org/10.1021/acs.chemmater.1c01274
[3] A.B. Kuznetsov, D.M. Ezhov, K.A. Kokh, N.G. Kononova, V.S. Shevchenko, S.V. Rashchenko, E.V. Pestryakov, V.A. Svetlichnyi, I.N. Lapin, A.E. Kokh. Mater. Res. Bull. **107**, 333 (2018). https://doi.org/10.1016/j.materresbull.2018.07.037
[4] Y. Shi, Z. Wang, Q. Ning, D. Wu, B. Quan. J. Mater. Sci.: Mater. Electr. **29**, *18*, 15894 (2018). https://doi.org/10.1007/s10854-018-9675-y
[5] X. Fan, X. Sun, C. Liu, W. Tian, M. Li, Y. Luo, C. Wu. J. Lumin. **242**, 118594 (2022). https://doi.org/10.1016/j.jlumin.2021.118594
[6] A.V. Ntarisa, D.J. Daniel, D. Balaji, A. Raja, H.J. Kim, N.D. Quang. J. Alloys. Compd. **873**, 159676 (2021). https://doi.org/10.1016/j.jallcom.2021.159676
[7] Y. Gao, C. Yin, P. Jiang, W. Gao, R. Cong, T. Yang. J. Solid State Chem. **293**, 121821 (2021). https://doi.org/10.1016/j.jssc.2020.121821
[8] Y. Gao, X. Zhu, H. Shi, P. Jiang, R. Cong, T. Yang. J. Lumin. **242**, 118598 (2022). https://doi.org/10.1016/j.jlumin.2021.118598
[9] L.M. Song, J.H. Gao, X.H. Yang, X.W. Huang, G.Q. Liu. Chin. J. Struct. Chem. **29**, *9*, 1309 (2010). https://www.researchgate.net/publication/286294952_Structure_and_Properties_of_a_New_Rare-earth_Borate_LiSrY2BO33
[10] P. Chen, M. Xia, R.K. Li. New J. Chem. **39**, **12**, 9389 (2015). https://doi.org/10.1039/C5NJ01913C
[11] H. He, Y. Qi, R. Cong, T. Yang. J. Solid State Chem. **301**, 122360 (2021). https://doi.org/10.1016/j.jssc.2021.122360
[12] K. Momma, F. Izumi. J. Appl. Crystallogr. **44**, *Part 6*, 1272 (2011). https://doi.org/10.1107/S0021889811038970
[13] G. Blasse. Phys. Lett. A **28**, *6*, 444 (1968). https://doi.org/10.1016/0375-9601(68)90486-6
[14] http://faculty.iitr.ac.in/ krjt8fcy/gocie.html